# The thermal decomposition of silver (I,III) oxide: A combined XRD, FT-IR and Raman spectroscopic study

**ARTICLE** *in* PHYSICAL CHEMISTRY CHEMICAL PHYSICS · JANUARY 2001

Impact Factor: 4.49 · DOI: 10.1039/b103226g



**3 AUTHORS**, INCLUDING:

Geoffrey I.N. Waterhouse
University of Auckland
**105** PUBLICATIONS **1,601** CITATIONS
SEE PROFILE

James B Metson
University of Auckland
**158** PUBLICATIONS **2,497** CITATIONS
SEE PROFILE

PCCP

# The thermal decomposition of silver (I, III) oxide: A combined XRD, FT-IR and Raman spectroscopic study

**Geoffrey I. N. Waterhouse, Graham A. Bowmaker and James B. Metson**

*Department of Chemistry, University of Auckland, Private Bag 90219, Auckland, New Zealand. E-mail: ga.bowmaker@auckland.ac.nz; Fax: 64 9 3737422; Tel: 64 9 3737599 Ext. 8303*

***Received 10th April 2001, Accepted 19th June 2001***
***First published as an Advance Article on the web 23rd July 2001***



FT-IR and Raman spectra for polycrystalline powders of silver (I, III) oxide, AgO, and silver (I) oxide, $Ag_2O$, are reported. The vibrational spectra for each oxide are discussed in relation to its crystal structure, and were found to be consistent with factor group analysis predictions. Infrared and Raman spectroscopy, in conjunction with powder XRD, were also used to follow the thermal decomposition of AgO powder in air. Supplementary studies employing differential scanning calorimetry (DSC) and temperature programmed reaction (TPR), provided additional information relevant to the decomposition process. In agreement with mechanisms previously reported, AgO was thermally reduced to metallic silver *via* two non-reversible steps, with the intermediate formation of $Ag_2O$. The transformation of AgO to $Ag_2O$ occurred with heating in the 373–473 K region, while the product of this reaction remained stable to temperatures in excess of 623 K. Complete thermal decomposition of the $Ag_2O$ intermediate to Ag and $O_2$ occurred at 673 K.

## Introduction

AgO and $Ag_2O$ are the two most thermodynamically stable oxides of silver. These materials have applications in many areas of technological importance. The most common usage of AgO is as a cathode material for zinc–silver oxide 'button cell' batteries, which provide the power source for many small electronic devices. These primary cells are characterised by a high energy output per unit weight, high discharge efficiency at approximately constant voltage ($\sim$1.5 V) and excellent shelf stability at room temperature.[1] The performance of Zn–AgO batteries deteriorates considerably with operation at elevated temperatures (above 323 K), due to internal complications arising from the thermal decomposition of the AgO cathode component. $Ag_2O$ is extensively utilised in the fields of heterogeneous catalysis and high performance materials science. Catalysts containing the bulk oxide, or those prepared using $Ag_2O$ as a precursor, are efficient for the decomposition of ozone[2,3] and halo-organic compounds.[4] Oxidation catalysts for carbon monoxide[5] and numerous other volatile organic compounds (VOCs),[6] based on $Ag_2O$, are also known. Thermally regenerable solid sorbents of $CO_2$ and $H_2O$ containing $Ag_2O$ have been developed for air-purification systems in aerospace vehicles.[7,8] The oxide is also used as an ionic modifier in fast-ion conducting glasses.[9] Furthermore, the physical and mechanical properties of hydroxyapatite bioceramics (synthetic bone) and $YBa_2Cu_3O_{7-x}$ superconductors prepared by the powder metallurgy route are improved when $Ag_2O$ is included in the fabrication process.[10–12]

Commercial interest in each of these technologies has motivated numerous studies examining the properties of AgO and $Ag_2O$, in particular their structure[13–20] and thermal stability.[21–25] A feature of the oxides less comprehensively documented is their vibrational spectra. AgO and $Ag_2O$, as with the other known oxides of silver, are materials poorly characterised by infrared and Raman spectroscopy. Few spectra for either compound are to be found in the literature. For the studies that been reported,[26–34] no detailed assignments or correlation with structure have been given. Thus, there exists a need for detailed infrared and Raman investigations of the two oxides.

The thermal decomposition of AgO in air represents an attractive process for study by vibrational spectroscopic methods. Changes in the vibrational spectra of AgO with increasing temperature can be used to follow both the decomposition mechanism and decomposition kinetics of the oxide. Such studies, combined with data obtained using conventional thermoanalytical methods, allow a more comprehensive model for the decomposition process to be established.

For these reasons, a comprehensive vibrational spectroscopic study of AgO and $Ag_2O$ was undertaken. The principal techniques employed were powder X-ray diffraction, FT-IR and Raman spectroscopy. The major objective of the work was to establish vibrational spectra–structure relationships for the two oxides through the application of factor group analysis. On the basis of this information, structural changes occurring during the thermal decomposition of AgO in air could then be monitored using the vibrational spectroscopic methods. Results presented are expected to find use in future research based on the oxides and their thermal decomposition products.

## Experimental

The AgO and $Ag_2O$ powders used in this work were prepared by chemical precipitation, in accordance with established procedures.[35,36] Analytical grade reagents, obtained from Aldrich, were used in each synthesis. Oxide powders were dried overnight at 328 K under a nitrogen gas purge. Prior to data acquisition, samples of $Ag_2O$ were annealed for 1 h at 473 K under a dry nitrogen purge to remove carbonate impurities formed through reaction of the oxide with atmospheric carbon dioxide.

Far-infrared measurements were performed on a Digilab FTS-60 series spectrometer, employing an FTS-60V vacuum optical bench with a 5 lines $mm^{-1}$ wire mesh beam splitter, a mercury lamp source and a pyroelectric triglycine sulfate

 DOI: 10.1039/b103226g

detector. Spectra were recorded at 2 $cm^{-1}$ resolution over the range 50–700 $cm^{-1}$ using 500 signal-averaged scans. Prior to data collection, the optical bench was evacuated to a pressure of $\sim 10^{-2}$ Torr. Mid-infrared studies on the same samples were carried out using a Digilab FTS-60 series spectrometer employing a DTGS detector. Acquisition parameters were: range, 400–2000 $cm^{-1}$; resolution, 2 $cm^{-1}$; with 500 scan co-addition. The spectra were obtained using pressed pellet samples. Fresh oxide (25–30 mg) was placed in a standard 13 mm die and compressed at a pressure of 1 ton $cm^{-2}$ to form a self-supporting disc of approximate thickness 0.05–0.10 mm. Pellets were mounted in a stainless steel disc holder for infrared experiments.

Raman studies of the oxide powders were performed by the rotating sample disk method, to minimise laser damage during data acquisition. Samples were prepared as thin discs (13 mm diameter, 1 mm thickness, 300 mg), and spun at 1500 r.p.m. during analysis. A commercially available 'spinning' cell (Jobin–Yvon) was used for this purpose, mounted in the macro-sampling compartment of a Jobin–Yvon U1000 Raman spectrometer. The spectrometer was equipped with an air-cooled photomultiplier tube (RCA-C31034A) and a standard photon counting module. Raman spectra were excited using 514.5 nm radiation from a Spectra-Physics $Ar^+$ laser (model 2017, 20 mW power). The incident angle of the laser beam on the surface of the rotating oxide pellet was 45°, and scattered light was collected perpendicular to the incident beam direction (90° sampling geometry). Spectra were collected over the range 50–1200 $cm^{-1}$, at 2 $cm^{-1}$ resolution. To improve the signal-to-noise ratio of the data reported, 10–15 scans recorded under similar conditions were co-added to produce a spectrum.

Powder X-ray diffraction patterns were acquired using a Phillips PW-1130 diffractometer, equipped with a Cu anode X-ray tube and curved graphite filter monochromator. Oxide samples were analysed without grinding, and were prepared for analysis by compaction into aluminium sample holders. XRD data was collected at room temperature, using monochromatised Cu-K$\alpha$ X-rays ($\lambda = 1.5418$ Å). Additional acquisition parameters were: $2\theta$ range, 25–50°; step size, 0.025°; and scan rate, 1.5° $min^{-1}$. Diffraction patterns were referenced against the JCPDS database for sample identification.

For FT-IR, Raman and XRD studies following the thermal decomposition of AgO in air, samples of fresh oxide were calcined for 1 h at selected temperatures between 295 and 873 K. A furnace preheated to the desired temperature was used for specimen heating. Following each heat treatment, samples were quickly cooled to room temperature under a dry nitrogen purge, then analysed by the three techniques.

The TPR experiment was performed in a continuous flow reactor, operated at atmospheric pressure with on-line mass spectrometric analysis of gaseous reaction products. The reactor consisted of a quartz U-tube cell mounted vertically within a temperature programmable furnace. AgO powder (25 mg) was loaded into the U-tube and supported on a porous quartz frit. A flow of helium carrier gas (20 mL $min^{-1}$) was passed through the cell, before the temperature was ramped from 295 to 873 K at a heating rate of 10 K $min^{-1}$. A K-type thermocouple positioned near the sample was used to monitor temperature during the heating program. The effluent stream was monitored for $O_2$, $CO_2$ and $H_2O$ using a quadrupole mass spectrometer (Balzers Thermocube). The temperature controller and mass spectrometer were both computer interfaced, permitting reaction temperature and evolved gas concentrations to be recorded simultaneously during the experiment.

Calorimetric data were obtained on a DSC-2 instrument (Rheometric Scientific Ltd.). AgO powder (10.0 mg) was weighed into an open aluminium crucible, and referenced against an empty Al crucible during measurements. DSC traces were recorded at a heating rate of 10 K $min^{-1}$, under a dry nitrogen purge.

Oxide morphology was examined using a Phillips XL-30 field emission scanning electron microscope (FESEM). Samples were mounted on aluminium sample stubs using double-sided adhesive tape. The electron gun was operated at an accelerating voltage of 12 kV for the collection of micrographs.

Specific surface areas were determined by the BET method, using krypton adsorption at 77 K. Adsorption studies were performed on a Quantasorb (Quantachrome), over the $P/P_o$ range 0.05–0.3. Samples (approx. 2 g) were outgassed overnight at 323 K prior to analysis. A value of 0.210 $nm^2$ was assumed for the cross-sectional area of the Kr molecule at liquid nitrogen temperature.

## Results and discussion

### Structural characterisation of the fresh oxides

The physical and structural properties of the freshly prepared $Ag_2O$ and AgO powders were examined by electron microscopy, powder X-ray diffraction and BET surface area measurement. Electron micrographs of the two oxides are shown in Fig. 1. The dark brown silver (I) oxide precipitate was characterised by a spherical grain morphology [Fig. 1(a)], with particle diameters between 0.5 and 2.0 μm. The X-ray diffraction pattern for this sample was indexed to that of the highly symmetric cubic $Ag_2O$ polymorph ($Pn\bar{3}m$). The BET surface area of the oxide was $0.493 \pm 0.001$ $m^2$ $g^{-1}$. AgO crystallised in the form of thin grey platelets of approximate thickness 0.2–0.5 μm, and diameter 0.5–3.0 μm [Fig. 1(b)]. The monoclinic silver (I, III) oxide polymorph ($P2_1/c$) was identified by XRD. The specific surface area of the micro-crystals was determined to be $0.411 \pm 0.001$ $m^2$ $g^{-1}$.

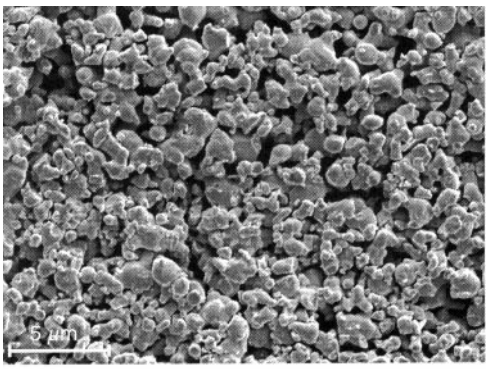


(a) $Ag_2O$

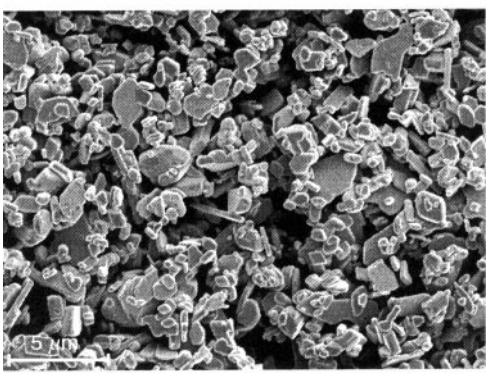


(b) AgO

**Fig. 1** SEM images of chemically prepared (a) $Ag_2O$ and (b) AgO. Both images were collected at the same magnification (× 10 000).

### Vibrational spectra of silver (I) oxide

The crystal structure of cubic $Ag_2O$ was first determined by Niggli *et al.*,[13] Davey[14] and Wycoff,[15] then later refined by Swanson.[16] The oxide was found to be isomorphous with cuprite, $Cu_2O$, and belongs to the space group $Pn\bar{3}m$ ($O_h^4$). The unit cell contains two formula units ($Z = 2$, $Ag_4O_2$). The structure consists of a face-centered cubic array of silver (I) ions interpenetrated by a body-centered cubic array of $O^{2-}$ ions. Monovalent silver ions are linearly coordinated by two $O^{2-}$ ions, and occupy the *b* lattice sites ($D_{3d}$ symmetry). The oxygen anions occupy the *a* lattice sites ($T_d$ symmetry) and are tetrahedrally coordinated by four silver cations. The shortest silver–oxygen bond distance in the structure is 2.05 Å,[16] considerably less than the sum of the ionic radii of the two ions (2.58 Å). Considerable covalent character in the bonding between the silver and oxygen ions of $Ag_2O$ accounts for the short Ag–O bond lengths observed, and also for the low coordination number of the Ag(I) ions. Ag $L_3$ X-ray absorption near-edge structure (XANES) studies have shown that Ag $4d_{z^2}$, 5s and 5p hybrid orbitals are involved in the chemical bonding within $Ag_2O$ and other oxidic compounds of silver containing Ag(I).[37,38]

Results of a factor group analysis performed for $Ag_2O$, based on the $O_h$ factor group, are given in Table 1. Also given is the contribution of each atom type to the overall vibrational degree of freedom ($\Gamma_{3N}$). The analysis predicts three optically active modes, consistent with previous theoretical predictions for the 'cuprite' structure.[39–41] $\Gamma_{vib} = A_{2u} + E_u + 2T_{1u}(IR) + T_{2u} + T_{2g}(R)$, where IR denotes infrared active and R denotes Raman active. Using mode descriptions reported for $Cu_2O$,[42] we can describe the nature of optically active phonons of $Ag_2O$. The infrared active modes ($T_{1u}$ symmetry) are associated with the relative motion of the silver and oxygen lattices, and are comprised of an asymmetric Ag–O stretching mode and an asymmetric O–Ag–O bending mode. The Raman active mode ($T_{2g}$ symmetry) involves the relative motion of $O^{2-}$ ions about a centre of symmetry at Ag(I), and is a symmetric Ag–O stretching vibration. Since the $Ag_2O$ structure has inversion symmetry, no optical mode exhibits both infrared and Raman activity.

The FT-IR absorbance spectrum of $Ag_2O$ powder, recorded at room temperature, is shown in Fig. 2(a). The spectrum contains six bands, centred at 86, 460(sh), 530, 565(sh), 650 and 951 $cm^{-1}$. For oxide pellets of the same density but different thickness, these bands were always observed with the same relative intensity. The Raman spectrum of $Ag_2O$ powder is shown in Fig. 3(a), and exhibits bands at 430(sh), 490, 711, 810 and 1068 $cm^{-1}$. We identify the bands at 711, 810 and 1068 $cm^{-1}$ with silver carbonate,[28,43] formed by reaction of the oxide with atmospheric carbon dioxide. The detection of carbonate in the Raman spectrum of $Ag_2O$ (and not in the infrared spectrum of the oxide) results from the long exposure time of the oxide pellet to the atmosphere during Raman data acquisition. No effort was made to protect the $Ag_2O$ pellet from atmospheric $CO_2$ during spectra collection. Also, the Raman technique may exhibit a greater surface sensitivity than infrared absorption spectroscopy, and so enhance the carbonate spectrum, since carbonate formation occurs at the surface of the $Ag_2O$ powder.

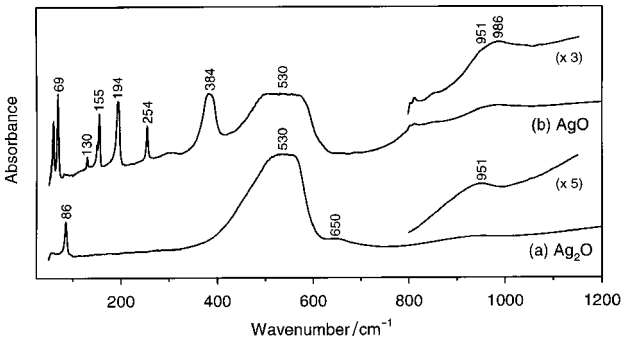


**Fig. 2** FT-IR absorbance spectra for chemically prepared (a) $Ag_2O$ and (b) AgO. Note that far-IR and mid-IR spectra have been combined and are presented as a single trace.

Previous studies have shown that $Ag_2O$ is characterised by two first-order infrared-active phonons, which at 298 K appear at 85 and 525–540 $cm^{-1}$.[28–30] The low frequency band is the $\delta_{as}$(O–Ag–O) bending mode, while the higher frequency band is the $\nu_{as}$(Ag–O) stretching mode. In the present study, the two strongest infrared absorption bands are observed at 86 and 530 $cm^{-1}$. On the basis of the close frequency correlation of these bands with those reported in the literature, we assign these features to the two zone-centre infrared active phonons ($T_{1u}$ symmetry) predicted by factor group analysis for

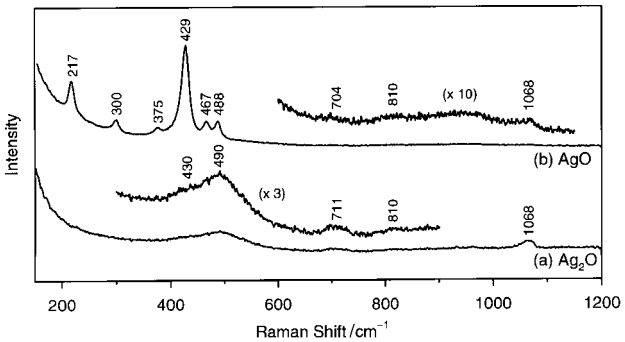


**Fig. 3** Raman spectra for chemically prepared (a) $Ag_2O$ and (b) AgO.

**Table 1** Crystallographic parameters and factor group analysis results for $Ag_2O$ and AgO

| Oxide | Crystallographic parameters[a] | Atom, site symmetry and multiplicity | | Transformation under factor group symmetry |
|---|---|---|---|---|
| $Ag_2O$ | $Pn\bar{3}m$ ($O_h^4$)<br>$Z = 2$ ($Ag_4O_2$)<br>$a_o = 4.736$ Å | Ag(I)<br>$O^{2-}$ | $D_{3d}$ (4)<br>$T_d$ (2) | $A_{2u} + E_u + 2T_{1u} + T_{2u}$<br>$T_{1u} + T_{2g}$<br>$\Gamma_{3N} = A_{2u} + E_u + 3T_{1u} + T_{2u} + T_{2g}$<br>$\Gamma_{acoustic} = T_{1u}$<br>$\Gamma_{vib} = A_{2u} + E_u + 2T_{1u} + T_{2u} + T_{2g}$ |
| AgO | $P2_1/c$ ($C_{2h}^5$)<br>$Z = 4$ ($Ag_4O_4$)<br>$a = 5.8592$ Å<br>$b = 3.4842$ Å<br>$c = 5.4995$ Å<br>$\beta = 107.506°$ | Ag(I)<br>Ag(III)<br>$O^{2-}$ | $C_i$ (2)<br>$C_i$ (2)<br>$C_1$ (4) | $3A_u + 3B_u$<br>$3A_u + 3B_u$<br>$3A_u + 3A_g + 3B_u + 3B_g$<br>$\Gamma_{3N} = 9A_u + 3A_g + 9B_u + 3B_g$<br>$\Gamma_{acoustic} = A_u + 2B_u$<br>$\Gamma_{vib} = 8A_u + 3A_g + 7B_u + 3B_g$ |

[a] Ref. 13–20.

the $Ag_2O$ structure. Both bands are considerably red-shifted relative to the corresponding bands for $Cu_2O$ (147 and 615 $cm^{-1}$, respectively),[29,44–49] as expected upon substitution of the heavier Ag(I) for Cu(I) in the $M_2O$ lattice (M = Cu, Ag).

The band at 530 $cm^{-1}$ is quite broad, and shows evidence of some splitting which is more evident when the spectrum is obtained at lower temperature (170 K). We attribute this structure to longitudinal optical–transverse optical (LO–TO) splitting, which may be observed in IR absorption spectra due to the occurrence of reflection of the incident radiation at grazing angles from the surface of the oxide particles. We propose that the lower and higher wavenumber shoulders at 460 and 565 $cm^{-1}$ arise through (LO–TO) splitting of the infrared-active $\nu_a$(Ag–O) mode of the oxide. Since $\nu_{LO} > \nu_{TO}$,[50] we assign the 460 $cm^{-1}$ band to the transverse optical mode of the Ag–O stretching mode, and that at 565 $cm^{-1}$ to the longitudinal component. Further justification for these assignments, based on a comparison with data for $Cu_2O$, is given below. The TO–LO splitting is not predicted on the basis of factor group analysis considerations, but satisfactorily explains why the infrared band arising through asymmetric Ag–O stretching vibration is so broad for the $Ag_2O$ powder. TO–LO splitting increases with increasing oscillator strength (larger dipole moment derivative, $\partial\mu/\partial Q$), and should be largest for the asymmetric Ag–O stretching mode of $Ag_2O$. For other modes of vibration, the splitting is typically small, within a few wavenumbers even for highly ionic oxide materials. Consistent with expectations, no splitting of the asymmetric O–Ag–O bending mode at 86 $cm^{-1}$ in the infrared spectrum of $Ag_2O$ was observed at room temperature.

Since only two infrared-active modes are predicted by theory for $Ag_2O$, the weaker bands appearing at 650 and 951 $cm^{-1}$ in the FT–IR spectrum of the oxide must arise through multi-phonon processes. McDevitt[30] reported that $Ag_2O$ is characterised by infrared bands at 540 and 645 $cm^{-1}$, although no assignment for the latter band was given. Infrared bands at 790 and 1125 $cm^{-1}$ reported for cuprous oxide, $Cu_2O$, are identified with combination modes of the optically active phonons.[48,49] Since $Ag_2O$ has the same crystallographic structure as $Cu_2O$, one would expect the two compounds to also exhibit similar vibrational spectra. For $Ag_2O$, the combination bands are expected at lower frequency than those reported for $Cu_2O$, since the optically active modes for the silver oxide are also of lower frequency. Observation of infrared bands at 650 and 951 $cm^{-1}$ for $Ag_2O$ accords favourably with this hypothesis. By analogy with reported literature for $Cu_2O$,[48,49] we assign these features to combination bands of the optically active phonons of $Ag_2O$. The origin of these combination bands is discussed below.

The Raman spectrum of $Ag_2O$ [Fig. 3(a)] contains a strong band at 490 $cm^{-1}$ with a weak shoulder at 430 $cm^{-1}$. Based on symmetry considerations, silver(I) oxide is predicted to have only a single Raman-active vibration of $T_{2g}$ symmetry. To explain the observation of the two bands, the high photosensitivity of the oxide must be considered. Recent literature suggests that the 490 $cm^{-1}$ band is characteristic for $Ag_2O$.[26,27] Millar *et al.*[27] observed two bands at 389 and 491 $cm^{-1}$ in the Raman spectrum of $Ag_2O$ powder. At higher laser powers, the intensity of the lower frequency band increased, whilst that of the 491 $cm^{-1}$ band diminished. It was proposed that the 491 $cm^{-1}$ band was characteristic for $Ag_2O$, and the 389 $cm^{-1}$ band was associated with products of laser irradiation. Ertl and coworkers[26] examined the thermal decomposition of the silver salt $Ag_7O_8NO_3$ under a nitrogen atmosphere. The salt is thermally reduced to AgO at temperatures above 373 K, and converted to $Ag_2O$ on heating at 473 K.[18] A band at 525 $cm^{-1}$ was assigned to a Raman vibration of $Ag_2O$. Nitrate ions from the parent oxide were noted at the oxide surface during data acquisition, which may have perturbed slightly the silver–oxygen stretching frequency for $Ag_2O$. The Raman-active phonon ($T_{2g}$ symmetry) of cuprous oxide is observed at 515 $cm^{-1}$ (15 K).[49] Due to the nature of the vibration, the frequency of the band should be relatively insensitive to the nature of the $M_2O$ cation. Thus, a similar vibrational frequency for this mode would be expected for both $Ag_2O$ and $Cu_2O$. The band at 490 $cm^{-1}$ observed in the present work is consistent with this theory, and is in reasonable agreement with the results of others.[26,27] Accordingly, we assign the 490 $cm^{-1}$ band to the Raman-active $\nu_s$(Ag–O) stretching mode of $Ag_2O$. The 430 $cm^{-1}$ band is attributed to a product of $Ag_2O$ photodecomposition during data collection.

Table 2 summarises the FT–IR and Raman data reported in this study for $Ag_2O$, and gives assignments for the observed spectral bands. Relevant data for $Cu_2O$ is also given for reference purposes. It can be shown that the 951 $cm^{-1}$ band in the infrared spectrum of $Ag_2O$ is of biphonic origin, and arises through combination of the Raman-active $\nu_s$(Ag–O) mode (490 $cm^{-1}$) with the IR-active transverse $\nu_{as}$(Ag–O) mode (460 $cm^{-1}$). Similarly, the 650 $cm^{-1}$ biphonon arises through combination of the infrared active phonon at 86 $cm^{-1}$ with the longitudinal $\nu_{as}$(Ag–O) mode (565 $cm^{-1}$). The TO–LO splitting observed here for the $\nu_{as}$(Ag–O) mode of $Ag_2O$ (105 $cm^{-1}$) is considerably larger than that reported for the same vibration in single crystal studies of $Cu_2O$ (29 $cm^{-1}$).[49] Differences in the magnitude of the splitting may be due to differences in M–O bond covalency between the two compounds. TO–LO splitting increases with increasing M–O bond ionicity, and may be as large as several hundred wavenumbers for highly ionic materials such as MgO.[50] The Cu–O bonding in cuprous oxide exhibits strong covalent character. Accordingly, the TO–LO splitting for this compound is small. The larger splitting observed in the present work for $Ag_2O$ suggests that Ag–O bonds may possess more ionic character than the Cu–O bonds of $Cu_2O$.

### Vibrational spectra of silver (I, III) oxide

AgO was originally thought to be isomorphous with CuO, containing bivalent Ag(II) ions. However, this structural model

**Table 2** Summarised vibrational data and band assignments for $Ag_2O$ and $Cu_2O$

| $Ag_2O$[a] | | $Cu_2O$[b] | | | |
|---|---|---|---|---|---|
| FT-IR $\nu$/$cm^{-1}$ | Raman $\nu$/$cm^{-1}$ | FT-IR $\nu$/$cm^{-1}$ | Raman $\nu$/$cm^{-1}$ | Symmetry assignment of phonons and combination band | Mode symmetry |
| 86 | | 146 | | $\Gamma_{15}^{-1}$ (TO) | $T_{1u}$ |
| | | 149 | | $\Gamma_{15}^{-1}$ (LO) | |
| | 490 | | 515 | $\Gamma_{25}^{+}$ | $T_{2g}$ |
| 460 | | 609 | | $\Gamma_{15}^{-2}$ (TO) | $T_{1u}$ |
| 565 | | 638 | | $\Gamma_{15}^{-2}$ (LO) | |
| 650 | | 790 | | $\Gamma_{15}^{-1}$ (LO) + $\Gamma_{15}^{-2}$ (LO) | combination |
| 951 | | 1125 | | $\Gamma_{15}^{-2}$ (TO) + $\Gamma_{25}^{+}$ | combination |

[a] This work. [b] Ref. 44–49.

was not consistent with the diamagnetic behaviour of the material. McMillan[17,18] was the first to propose that AgO was a mixed valence compound, containing an equal number of Ag(I) and Ag(III) cations. The empirical formula AgO is somewhat misleading, and the oxide is more accurately described as $Ag^{I}Ag^{III}O_2$. The crystallographic structure of monoclinic AgO has been determined by X-ray[17–19] and neutron diffraction[20] methods. The oxide belongs to the space group $P2_1/c$ ($C_{2h}^5$), with primitive cell formula $Ag_4O_4$. The structure consists of a distorted face-centred cubic arrangement of metal ions, with monovalent Ag(I) cations linearly coordinated by two oxygen anions, and trivalent Ag(III) cations approximately square-planar coordinated by four oxygen anions. The square-planar geometry at Ag(III) is typical for transition metal ions with the $nd^8$ electron valence configuration. Each oxygen atom is coordinated by two Ag(III) cations and one Ag(I) cation, and the bonding geometry at oxygen is approximately trigonal pyramidal. Two Ag–O bond distances are present in the structure, 2.18 and 2.03 Å. The first corresponds to the linear bonds about Ag(I), the second to the square-planar bonding of Ag(III). Differences in the two bond lengths are consistent with Ag(III) ions having a smaller ionic radius than Ag(I) ions. As with $Ag_2O$, the short Ag–O bond lengths reflect the covalent character of the bonding within the oxide. Ref. 51 provides a more comprehensive description of the bonding in AgO.

A factor group analysis was carried out to establish the nature of the optically active vibrational modes for monoclinic AgO. Results of the vibrational analysis are given in Table 1. The study was carried out under the $C_{2h}$ factor group with the two Ag(III) ions and two Ag(I) ions of the primitive cell in sites of $C_i$ symmetry, and the four $O^{2-}$ ions in $C_1$ sites. The analysis yields $\Gamma_{vib} = 8A_u(IR) + 7B_u(IR) + 3A_g(R) + 3B_g(R)$. Thus the monoclinic AgO polymorph is predicted to give rise to 21 optically active modes, 15 of which are infrared active ($8A_u + 7B_u$) and 6 of which are Raman active ($3A_g + 3B_g$). No IR/R coincidences occur since the $C_{2h}$ point group has inversion symmetry. Note that the number of optically active modes predicted for AgO is considerably higher than that of $Ag_2O$, consistent with the lower point group symmetry of the AgO lattice and the greater number of atoms in the primitive cell.

The FT-IR absorption spectrum of freshly prepared AgO powder is shown in Fig. 2(b). Bands identified with the oxide occur at the following frequencies: 60, 69, 130, 150, 155, 194, 254, 384, 530, 951 and 986 $cm^{-1}$. The feature at 86 $cm^{-1}$ is due to an $Ag_2O$ impurity, produced during the drying process of the AgO powder following precipitation. Weak bands at 300, 710, 720, 785, 800 and 1071 $cm^{-1}$ are characteristic of silver carbonate.[28,43] Removal of the carbonate by sample calcination prior to the analysis was not possible, since the thermal stability of AgO[22–25] is lower than that of $Ag_2CO_3$.[52] However, silver carbonate is well characterised by vibrational spectroscopy and bands attributable to the impurity were easily distinguished from those of AgO. The intense band at 530 $cm^{-1}$ is characteristic of Ag(I) ions linearly coordinated by two oxygen anions, as is observed in the infrared spectrum of $Ag_2O$. We identify the band with the $\nu_{as}$(Ag–O) mode of such linkages in the AgO lattice.

In order to assign features of the vibrational spectra of AgO arising from vibrations of the square-planar '$Ag^{III}O_4$' unit, it is helpful to consider the normal vibrational modes of square-planar ions of the type $MX_4^{n-}$. $AuCl_4^-$ and $PdCl_4^{2-}$ are examples of this type of species. The free $MX_4^{n-}$ ion belongs to the $D_{4h}$ point group, and gives rise to seven fundamental modes of vibration. These seven modes, their symmetry assignments and activities are listed in Table 3. The normal modes of vibration of the '$Ag^{III}O_4$' unit in AgO are expected to be similar to those of $MX_4^{n-}$, except that the Ag(III) cations will occupy sites of $C_i$ symmetry rather than $D_{4h}$. The effect of lowering the site symmetry at the metal is to lift the degeneracy of the two infrared-active modes of $E_u$ symmetry ($\nu_6$ and $\nu_7$). Thus, the '$Ag^{III}O_4$' unit will exhibit two vibrations of $A_u$ symmetry for both $\nu_6$ and $\nu_7$. The higher frequency of these two is $\nu_6$, the Ag–O stretching mode of the '$Ag^{III}O_4$' units. Apart from the strong band at 530 $cm^{-1}$ already assigned to the Ag–O stretch of the '$Ag^{I}O_2$' units, the highest frequency band occurs at 384 $cm^{-1}$, and this is assigned to one of the two Ag–O bands expected for the '$Ag^{III}O_4$' units. The second must lie above the 384 $cm^{-1}$ band, otherwise the average frequency of the $Ag^{III}O_4$ units would be too far below that of the $Ag^{I}O_2$ units (a lowering of the M–O stretching frequency with increasing coordination number at a metal centre is common for many transition metal oxides, but this effect will be compensated by the increase in oxidation state of the silver cation from +1 to +3). Also, the intensity of the second band should be comparable to that of the 384 $cm^{-1}$ band, as these two bands arise from site group splitting of a doubly degenerate Ag–O mode of the approximately $D_{4h}$ '$Ag^{III}O_4$' unit. Therefore, the only reasonable location for this band is within the envelope of the broad band at 530 $cm^{-1}$. A shoulder at 502 $cm^{-1}$, which disappears when the AgO is thermally decomposed to $Ag_2O$ (see below), is therefore tentatively identified as the second component of the two $\nu_d$(Ag–O) modes expected for the '$Ag^{III}O_4$' unit (Table 3).

**Table 3** Vibrational data and band assignments for the square-planar '$Ag^{III}O_4$' unit of AgO

| $MX_4^{n-}$ ($D_{4h}$) | '$Ag^{III}O_4$' ($C_i$) | Assignment | AgO /$cm^{-1}$ |
|---|---|---|---|
| Raman-active | | | |
| $A_{1g}$ | $A_g$ | $\nu_1$, $\nu_s$(Ag–O) | 429 |
| $B_{1g}$ | $A_g$ | $\nu_2$, $\delta_s$($AgO_2$) | 217 |
| $B_{2g}$ | $A_g$ | $\nu_4$, $\nu_a$(Ag–O) | 467 |
| Infrared-active | | | |
| $E_u$ | $A_u$ | $\nu_6$, $\nu_d$(Ag–O) | 502? |
| | $A_u$ | | 384 |
| $E_u$ | $A_u$ | $\nu_7$, $\delta_d$($AgO_2$) | — |
| | $A_u$ | | |
| $A_{2u}$ | $A_u$ | $\nu_3$, out-of-plane bend | — |
| Inactive | | | |
| $B_{2u}$ | $A_u$ | $\nu_5$, out-of-plane bend | — |

The infrared bands at 951 and 986 $cm^{-1}$ probably arise through combination of the Raman-active and infrared-active silver–oxygen stretching fundamentals of AgO (429 + 530 = 959, 467 + 530 = 997). IR bands below 300 $cm^{-1}$ are associated with other vibrational modes of the AgO lattice, in particular bending and deformation vibrations. Fewer fundamental infrared active bands were observed for the oxide than are predicted by theory. Bands not identified here may either be very weak, or obscured by other bands.

The Raman spectrum of AgO [Fig. 3(b)] contains six sharp bands, at frequencies 217, 300, 375, 429, 467 and 488 $cm^{-1}$. The position and intensities of these bands correlate favourably with reported data for monoclinic AgO prepared by electrochemical methods.[31–34] The observation of six Raman active bands is consistent with the factor group analysis predictions for the oxide [$3A_g(R) + 3B_g(R)$]. These bands are associated with the motions of oxygen anions in the AgO lattice, since the six irreducible representations arise through the transformation of $O^{2-}$ ions under the $C_{2h}$ factor group (see Table 1). Additional bands due to silver carbonate were observed in the 600–1100 $cm^{-1}$ region [Fig. 3(b), expanded view].

The band at 488 $cm^{-1}$ is of similar frequency and intensity to the band at 490 $cm^{-1}$ in the Raman spectrum of $Ag_2O$. Accordingly, we assign these bands to the $\nu_s$(Ag–O) mode for Ag(I) cations linearly coordinated by oxygen in the AgO structure. Information from Table 3 was used to assign Raman

bands arising from the square-planar '$Ag^{III}O_4$' unit. To a simple approximation, the '$Ag^{III}O_4$' unit is expected to give rise to three Raman-active modes; a symmetric Ag–O stretching vibration ($\nu_1$), an asymmetric stretching vibration ($\nu_4$) and a symmetric bending vibration ($\nu_2$). Bosworth and Clark[53] measured the intensity of the Raman active fundamentals for a number of square-planar ions of the type $MX_4^{n-}$, and calculated bond polarisabilities and bond anisotropies. For all ions, the totally symmetric M–X stretching vibration ($\nu_1$) gave rise to the most intense Raman band. On this basis, we assign the intense peak at 429 $cm^{-1}$ in the Raman spectrum of AgO to the $\nu_s$(Ag–O) mode for oxygen square-coordinated about Ag(III). The frequency of the band is in the region expected for a Ag–O stretching vibration, and lower than that observed for the same vibration of linearly coordinated Ag(I).

The weak band at 467 $cm^{-1}$ is assigned to the Raman-active asymmetric stretching mode ($\nu_4$) predicted for the '$Ag^{III}O_4$' unit. The band at 217 $cm^{-1}$ is assigned to the symmetric bending mode ($\nu_7$) of the '$Ag^{III}O_4$' unit. For $MX_4^{n-}$ ions, the band is of medium Raman intensity, and is observed at approximately one-half the frequency of the symmetric M–X stretching mode.[53] These observations are consistent with the properties of the 217 $cm^{-1}$ band. No assignment is given for the weak bands at 300 and 375 $cm^{-1}$.

### The thermal decomposition of silver (I, III) oxide in air

The thermal decomposition of AgO in air has been studied by several research groups.[23–25] The decomposition kinetics are known to be highly dependent on the method of oxide preparation (chemical or electrochemical) and on the mechanical processing history of the sample.[25] To gauge the thermal stability and purity of the AgO powder used in this work, preliminary TPR and DSC studies of the material were performed. Results obtained using these conventional thermoanalytical techniques are presented in Fig. 4, and provide a useful basis for subsequent investigations examining the thermal decomposition of the oxide by XRD, FT-IR and Raman spectroscopy.

Fig. 4(a) shows the $O_2$-TPR spectrum for AgO, which features two dioxygen evolution signals at 468 and 727 K. The areas beneath the two signals are approximately equal, indicating that equivalent amounts of $O_2$ were evolved during each separate thermal event. Small amounts of carbon dioxide and water were evolved at 453–483 K during the TPR experiment, attributable to the decomposition of simple and basic carbonate impurities.[52] Areas for these signals were less than 3% of the oxygen signals. The temperature of the first $O_2$ evolution signal coincides with a complex transition in the DSC trace for the oxide [Fig. 4(b)]. An expanded view of this region is provided. Three component features are observed: a small exothermic peak at 392 K, an endothermic peak at 441 K followed immediately by an exothermic peak at 468 K. The latter peak we associate with the thermal decomposition of AgO to $Ag_2O$, since $O_2$ was evolved at the same temperature. The two peaks at lower temperature presumably involve some form of structural modification within the AgO lattice prior to decomposition, as no oxygen, carbon dioxide or water evolution accompanied these features. The $O_2$ evolution signal at 727 K coincides with a strong endothermic DSC transition at the same temperature. We correlate both these features with the thermal decomposition of $Ag_2O$ to its component elements.

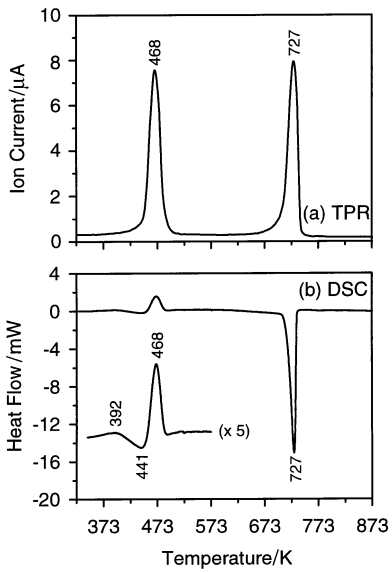


**Fig. 4** (a) TPR and (b) DSC curves for chemically prepared AgO. The heating rate used in both studies was 10 K $min^{-1}$.

The results reported here accord favourably with previous literature relating to the thermal stability of chemically precipitated AgO powders,[22–25] and support the established mechanism given by eqn. (1) and (2) for the thermal decomposition of AgO.

$$Ag^{I}Ag^{III}O_2(s) \xrightarrow{T>373\ K} Ag_2O(s) + 0.5\,O_2(g) \quad (1)$$

$$Ag_2O(s) \xrightarrow{T>623\ K} 2Ag(s) + 0.5\,O_2(g) \quad (2)$$

Reported activation energies for reactions (1) and (2) in air at atmospheric pressure are 132.6 and 283.4 kJ $mol^{-1}$, respectively.[23]

Structural changes occurring during the thermal decomposition of AgO in dry air were followed by powder X-ray diffraction. Fig. 5 shows XRD patterns for fresh oxide samples calcined for 1 h at the temperatures indicated. Data were collected at room temperature, following sample cooling under a nitrogen atmosphere. Sample annealed at 373 K gave rise to the same powder pattern as the freshly prepared oxide, characteristic for monoclinic AgO [Fig. 5(a)]. At temperatures above 393 K, reflections attributable to $Ag_2O$ ($2\theta = 32.8$, 38.2°) began to appear, while those of AgO were proportionally attenuated [Fig. 5(b), (c)]. The diffraction pattern obtained following sample heating at 473 K [Fig. 5(d)] was that of cubic $Ag_2O$, indicating that the complete thermal reduction of AgO to $Ag_2O$ was effected by this treatment. The colour change of the sample from grey (AgO) to dark brown

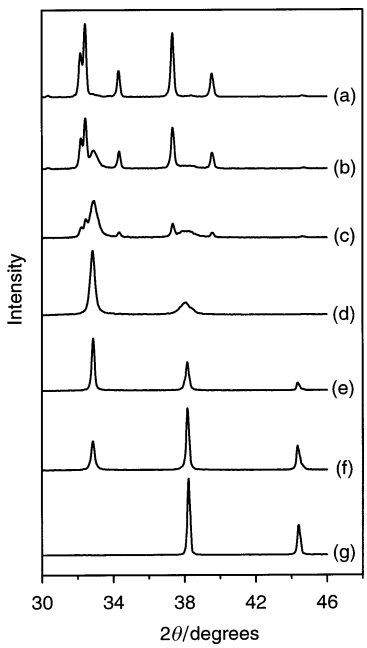


**Fig. 5** Powder XRD patterns for AgO samples calcined for 1 h under isothermal conditions at (a) 373; (b) 413; (c) 433; (d) 473; (e) 623; (f) 648 and (g) 673 K.

($Ag_2O$) with the 473 K anneal provided qualitative support for this transformation. After heating at 623 K [Fig. 5(e)], the formation of metallic silver commenced ($2\theta = 38.2$, 44.3°) whilst the $Ag_2O$ reflections lost intensity. Silver was the only phase identified after sample calcination at 673 K [Fig. 5(g)].

Onset temperatures for reactions (1) and (2) determined by XRD were considerably lower than the corresponding values measured using TPR and DSC. The nature of the heating programs used to obtain each set of data is responsible for this discord. TPR and DSC are dynamic heating methods, and accordingly exhibit a non-immediate thermal response. Due to this thermal lag, sample transitions are registered at higher temperatures than studies employing an isothermal, stepwise program like that used here for XRD and subsequent FT-IR/Raman studies. If all experiments had been performed using the same heating regime, either dynamic or stepwise isothermal, the transition temperatures reported would be in closer agreement.

Far-infrared absorbance spectra for AgO samples calcined in an identical manner to those used in the XRD study are presented in Fig. 6. The spectrum obtained following sample treatment at 373 K was that of monoclinic AgO [Fig. 6(a)]. With heating to successively higher temperatures between 393–453 K [Fig. 6(b), (c)], bands characteristic of the parent oxide (except that at 530 $cm^{-1}$) lost intensity while additional bands at 86 $cm^{-1}$ and 650 $cm^{-1}$ developed. The 530 $cm^{-1}$ band gained intensity with the higher temperature treatments. The spectrum obtained after sample calcination at 473 K [Fig. 6(d)] was indistinguishable from that of chemically prepared $Ag_2O$ and exhibited characteristic maxima at 86, 530 and 650 $cm^{-1}$.

The thermal decomposition of $Ag_2O$ to metallic silver occurred between 623 and 673 K, as evidenced by the progressive attenuation of bands typical for the oxide with increasing temperature in this range [Fig. 6(e)–(g)]. The thin silver pellet obtained by the thermal reduction of the oxide exhibited no infrared absorption.

Raman spectra documenting the thermal decomposition of AgO in air are displayed in Fig. 7. Samples of fresh AgO were calcined for 1 h at the temperatures indicated, then cooled to room temperature for analysis. Fig. 7(f) was obtained following sample heating for 5 h in air at 873 K. The Raman spectrum of the sample annealed at 373 K [Fig. 7(a)] was typical

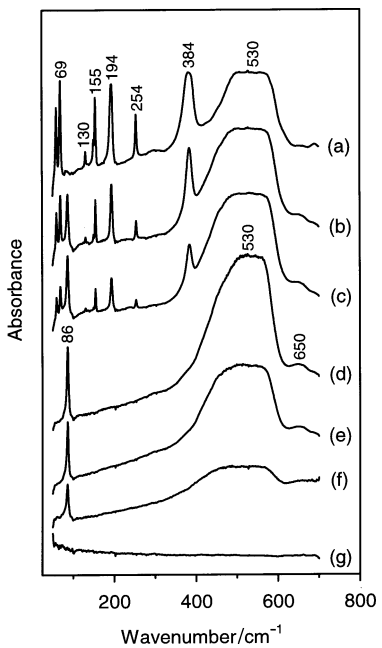


**Fig. 6** FT-IR absorbance spectra for AgO samples calcined for 1 h under isothermal conditions at (a) 373; (b) 413; (c) 433; (d) 473; (e) 623; (f) 648 and (g) 673 K.

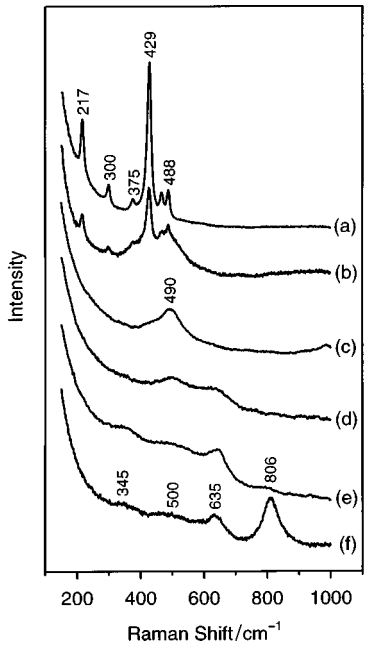


**Fig. 7** Raman spectra for AgO samples calcined for 1 h under isothermal conditions at (a) 373; (b) 423; (c) 473; (d) 623; (e) 673 and (f) 873 K (5 h).

of monoclinic AgO, comprised of six sharp bands at 217, 300, 375, 429, 467 and 488 $cm^{-1}$. With increasing temperature in the range 373–473 K [Fig. 7(b), (c)], bands characteristic of AgO lost intensity and were replaced progressively by a broad feature at 490 $cm^{-1}$. We identify this low intensity band with the $\nu_s$(Ag–O) mode of $Ag_2O$. These spectra demonstrate that the structural transformation of AgO to $Ag_2O$ was effected with sample heating in air from 373 to 473 K, consistent with the findings of our earlier XRD and FT-IR studies.

Some metallisation at the surface of the oxide pellet was observed following sample calcination at 623 K [Fig. 7(d)], which reduced the intensity of the $Ag_2O$ band at 490 $cm^{-1}$ considerably. The development of a weak feature at 635 $cm^{-1}$ also accompanied this treatment. Heating at 673 K [Fig. 7(e)] decomposed the remaining $Ag_2O$ to elemental silver, evidenced spectroscopically by the disappearance of the 490 $cm^{-1}$ band characteristic for silver (I) oxide. The metallic appearance of all samples calcined above 673 K provided qualitative support for this structural transformation. Spectra collected from samples heated in air at 673 K [Fig. 7(e)] contained bands at 345, 500 and 635 $cm^{-1}$, while an additional feature at 806 $cm^{-1}$ emerged with prolonged sample calcination at 873 K [Fig. 7(f)]. We identify these bands with vibrational modes of several different oxygen species adsorbed on silver.[26,54–58]

## Conclusions

FT-IR and Raman spectroscopy, used in conjunction with powder X-ray diffraction, were applied successfully to the characterisation of the silver oxides, AgO and $Ag_2O$. Vibrational spectra for both oxides were in accordance with factor group analysis predictions based on their structure. The vibrational techniques also provided direct information about the chemical and structural transformations occurring during the thermal decomposition of AgO in air. The decomposition of AgO to metallic silver was observed to proceed *via* an $Ag_2O$ intermediate.

## References

1 G. R. Graybill, R. K. Grubbs, J. A. Gucinski and D. F. Smith, *J. Power Sources*, 1997, **65**, 47.
2 S. Imamura, M. Ikebata, T. Ito and T. Ogita, *Ind. Eng. Chem. Res.*, 1991, **30**, 217.

3 B. Dhandapani and S. T. Oyama, *Appl. Catal. B*, 1997, **11**, 129.
4 K. Kiyono and K. Shiragami, *Jpn. Pat*., 10 099 646, 1998.
5 E. Gulari, C. Guldur, S. Osuwan and S. Srivannavit, *Appl. Catal. A*, 1999, **182**, 147.
6 M. Luo, X. Yuan and X. Zheng, *Appl. Catal. A*, 1998, **175**, 121.
7 P. J. Birbara and T. A. Nalette, *US Pat*., 5 174 974, 1992.
8 J. R. Aylward, P. J. Birbara and T. A. Nalette, *US Pat*., 5 427 751, 1995.
9 A. Abousehly, R. El-mallaway and E. Yousef, *J. Mater. Sci. Lett*., 2000, **19**, 409.
10 I. Manjubala and T. S. Sampath Kumar, *Biomaterials*, 2000, **21**, 1995.
11 A. Kumar, K. Mallick, S. Samajar, S. K. Samanta and K. Shyam, *J. Mater. Sci. Lett*., 1990, **9**, 137.
12 S. Samajar and S. K. Samanta, *J. Mater. Sci*., 1992, **27**, 4709.
13 P. Niggli, *Z. Kristallogr*., 1922, **57**, 252.
14 W. P. Davey, *Phys. Rev*., 1922, **19**, 248.
15 R. W. G. Wyckoff, *Am. J. Sci*., 1922, **3**, 184.
16 E. H. Evans, M. C. Morris, R. P. Stinchfield and H. E. Swanson, *U.S. Natl. Bur. Stand*., 1962, Monograph 25.
17 J. A. McMillan, *J. Inorg. Nucl. Chem*., 1960, **13**, 28.
18 J. A. McMillan, *Chem. Rev*., 1962, **62**, 65.
19 M. Fischer and M. Jansen, *J. Less-Common Met*., 1988, **137**, 123.
20 N. E. Brese, M. O'Keeffe, B. L. Ramakrishna and R. B. Von Dreele, *J. Solid State Chem*., 1990, **89**, 184.
21 B. V. L'vov, *Thermochim. Acta*, 1999, **333**, 13.
22 H. T. Spath, K. Torkar and H. G. Winkler, *Proceedings of the 7th International Symposium on the Reactivity of Solids*, Chapman and Hall, London, 1972, p. 745.
23 H. J. Chuang and H. W. Ko, *Proc. Natl. Sci. Counc. ROC* (*A*), 1989, **13**, 145.
24 S. Dallek, B. F. Larrick and W. A. West, *J. Electrochem. Soc*., 1986, **133**, 2451.
25 K. Takeda, *J. Electrochem. Soc*., 1996, **143**, 418.
26 X. Bao, G. Ertl, M. Muhler, B. Pettinger, R. Schlogl and I. C. Wilcock, *Angew. Chem. Int. Ed. Engl*., 1994, **33**, 85.
27 G. J. Millar, M. L. Nelson and P. J. R. Unwins, *Catal. Lett*., 1997, **43**, 97.
28 R. G. Greenler, B. J. Lindgren, A. J. Mallmann and T. L. Slager, *J. Phys. Chem*., 1972, **76**, 940.
29 N. T. McDevitt and A. D. Davidson, *J. Opt. Soc*., 1965, **55**, 209.
30 W. L. Baun and N. T. McDevitt, *Spectrochim. Acta*, 1964, **20**, 799.
31 R. Kotz and E. Yeager, *J. Electroanal. Chem*., 1980, **111**, 105.
32 S. Huang, Z. Jiang and B. Qian, *Electrochim. Acta*, 1994, **39**, 2465.
33 G. I. Lacconi, O. Sala and M. L. A. Temperini, *J. Electroanal. Chem*., 1987, **227**, 21.
34 N. Iwasaki, Y. Nishina and Y. Sasaki, *Surf. Sci*., 1988, **198**, 524.
35 R. N. Hammer and J. Kleinberg, *Inorg. Synth*., 1953, **4**, 12.
36 J. A. Allen and P. H. Scaife, *Aust. J. Chem*., 1966, **19**, 715.
37 P. Behrens, *Solid State Commun*., 1992, **81**, 235.
38 P. Behrens, S. Assmann, U. Bilow, C. Linke and M. Jansen, *Z. Anorg. Allg. Chem*., 1999, **625**, 111.
39 K. Huang, *Z. Phys*., 1963, **171**, 213.
40 C. Carabatos and C. Rendus, *Acad. Sci. Paris*, 1970, **270**, 1289.
41 C. Carabatos and B. Prevot, *Phys. Status Solidi*, 1970, **37**, 773.
42 R. J. Elliot, *Phys. Rev*., 1961, **124**, 340.
43 K. Aoki and T. Morimoto, *Langmuir*, 1986, **2**, 525.
44 M. Terada, *Bull. Chem. Soc. Jpn*., 1964, **20**, 809.
45 E. C. Heltemes, *Phys. Rev*., 1966, **141**, 803.
46 B. Hejda and J. Pastrnak, *Phys. Status Solidi A*, 1972, **10**, 487.
47 J. C. W. Taylor and F. L. Weichman, *Can. J. Phys*., 1971, **49**, 601.
48 R. Becker, V. M. Burlakov, M. Goppert, A. Jolk and C. F. Klingshirn, *Phys. Lett. A*, 1999, **254**, 95.
49 A. Endriss, J. Ihringer, M. Ivanda, W. Kiefer, A. Kirfel and D. Waasmaier, *J. Raman Spectrosc*., 1997, **28**, 487.
50 G. Busca, *Catal. Today*, 1996, **27**, 323.
51 A. J. Salkind, in *Zinc–Silver Oxide Batteries*, *Pap. Symp*., Wiley, New York, 1971, ch. 9, p. 107.
52 Y. Sawada and K. Manabe, *J. Therm. Anal*., 1991, **37**, 1657.
53 Y. M. Bosworth and R. J. H. Clark, *Inorg. Chem*., 1975, **14**, 170.
54 G. A. Bowmaker, R. P. Cooney, J. B. Metson and G. A. Millar, *J. Chem. Soc., Faraday Trans*., 1995, **91**, 4149.
55 X. Bao, G. Ertl, M. Muhler, B. Pettinger and I. C. Wilcock, *Phys. Rev. Lett*., 1994, **72**, 1561.
56 X. Bao, G. Ertl, G. Lehmpfuhl, M. Muhler, B. Pettinger, R. Schlogl and Y. Uchida, *Catal. Lett*., 1995, **32**, 171.
57 X. Bao, G. Ertl, B. Pettinger and R. Schlogl, *Ber. Bunsen-Ges. Phys. Chem*., 1993, **97**, 322.
58 G. I. N. Waterhouse, G. A. Bowmaker and J. B. Metson, in preparation